7

Torsion

In the previous chapters, the behavior of beams subjected to axial and transverse loads is studied in detail. In chapter 6, a fairly general, three dimensional loading is considered, with one important restriction: the beam is assumed to *bend without twisting*. Twisting, however, is often present in structures, and in fact, many important structural components are designed to carry torsional loads primarily.

Power transmission drive shafts are a prime example of structural components designed to carry a specific torque. Such components are designed with solid or thin-walled circular cross-sections. Numerous other structural components are designed to carry a combination of axial, bending, and torsional loads. For instance, an aircraft wing must carry the bending and torsional moments generated by the aerodynamic forces.

The behavior of structural components under torsional loads is the subject of this chapter. The focus is on long prismatic structures similar to the beams treated in the two previous chapters. When a long prismatic structure is subjected to torsion, it is often referred to as a "bar" rather than a "beam," but the two terms are often used interchangeably.

7.1 Torsion of circular cylinders

Consider an infinitely long, homogeneous, solid or hollow circular cylinder subjected to end torques, Q_1, of equal magnitude and opposite directions, as depicted in fig. 7.1. The cross-section of the cylinder can be a circle of radius R, or a circular annulus of inner and outer radii, R_i and R_o, respectively.

This problem is characterized by two types of symmetries. First, a cylindrical symmetry about axis $\bar{\imath}_1$: any rotation of the cylinder or tube about axis $\bar{\imath}_1$ leaves both the structure and the loading unchanged, and hence, the solution must remain unchanged. Second, as illustrated in fig. 7.2, the cylindrical structure is symmetric with respect to any plane, $\mathcal{P}$, passing through axis $\bar{\imath}_1$. Depicted on this figure are two points, **A** and **B**, both on a circle, $\mathcal{C}$, of radius $r < R$. The plane of symmetry, $\mathcal{P}$, is selected to be normal to the line segment joining these two points. Along circle $\mathcal{C}$,

shear stresses will develop stemming from the application of torque Q_1. Because of the circular symmetry of the system, this shear stress must be of constant magnitude along circle $\mathcal{C}$, and tangent to it at all points. While the structure is *symmetric* with respect to plane $\mathcal{P}$, the loading is *antisymmetric* with respect to the same plane. Consequently, the solution must be antisymmetric with respect to plane $\mathcal{P}$.

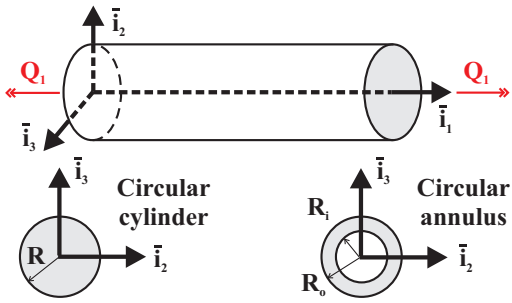

Fig. 7.1. Circular cylinder subjected to end torques.

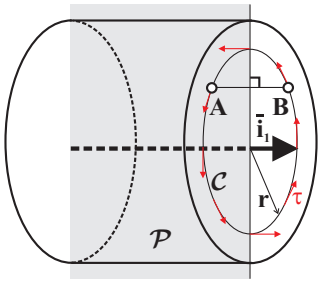

Fig. 7.2. A plane of symmetry, $\mathcal{P}$, of the circular cylinder.

First, consider the axial displacement components at points **A** and **B**, denoted u_1^A and u_1^B, respectively. The cylindrical symmetry of the problem implies that $u_1^A = u_1^B$. On the other hand, the antisymmetry of the problem with respect to plane $\mathcal{P}$ implies $u_1^A = -u_1^B$. The only solution consistent with these two requirements is $u_1^A = u_1^B = 0$. Because points **A** and **B** are arbitrary points on the cross-section, the axial displacement must vanish at all points of the cross-section: *the cross-section does not warp out-of-plane*.

Next, consider the in-plane displacements of the same two points. The only displacement field that is compatible with the cylindrical symmetry of the problem is a rigid body rotation of the cross-section about its own center. It is easy to show that this rigid body rotation also presents the required antisymmetry about any plane passing through axis $\bar{\imath}_1$.

In summary, for a circular cylinder or annulus, each cross-section *rotates about its own center like a rigid disk*. This is the only deformation compatible with the symmetries of the problem.

7.1.1 Kinematic description

Since the only deformation induced by torsion in a circular cylinder or annulus consists of rigid body rotation of each cross-section, its motion is fully described by a rotation angle, Φ_1, as shown in fig. 7.3. This rotation brings an arbitrary point **A** of the reference configuration to point $\mathbf{A}'$ in the deformed configuration. Figure 7.3 also shows polar coordinates r and α that define the position of point **A**. As usual, displacement, and rotations are assumed to remain small, and hence, the distance from

A to **A**′ can be approximated as $r\,\mathrm{d}\Phi_1$, as shown in the figure. The sectional in-plane displacement field can then be written as the projection of this displacement vector along directions $\bar{\imath}_2$ and $\bar{\imath}_3$, respectively, to find

$$u_2(x_1, r, \alpha) = -r\Phi_1(x_1)\sin\alpha, \quad u_3(x_1, r, \alpha) = r\Phi_1(x_1)\cos\alpha. \tag{7.1}$$

Because the cross-section does not deform out of its own plane, the axial displacement field must vanish, *i.e.*, $u_1(x_1, x_2, x_3) = 0$.

The out-of-plane displacement field describing the torsional deformation of the circular cylinder becomes

$$u_1(x_1, x_2, x_3) = 0, \tag{7.2}$$

whereas the in-plane displacement field given by eq. (7.1) becomes

$$\begin{aligned} u_2(x_1, x_2, x_3) &= -x_3\Phi_1(x_1), \\ u_3(x_1, x_2, x_3) &= x_2\Phi_1(x_1), \end{aligned} \tag{7.3}$$

where the following transformation from polar to Cartesian coordinates is used: $x_2 = r\cos\alpha$ and $x_3 = r\sin\alpha$.

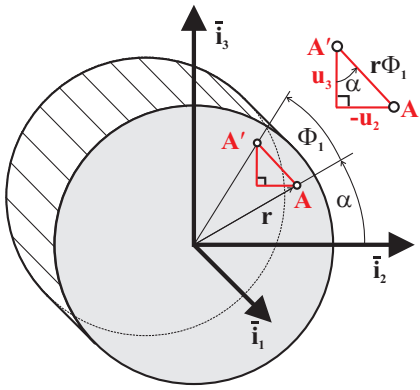

Fig. 7.3. In-plane displacements for a circular cylinder. The cross-section undergoes a rigid body rotation.

Using the strain-displacement relationships, the corresponding strain field is now obtained as

$$\epsilon_1 = \frac{\partial u_1}{\partial x_1} = 0, \tag{7.4}$$

$$\epsilon_2 = \frac{\partial u_2}{\partial x_2} = 0, \quad \epsilon_3 = \frac{\partial u_3}{\partial x_3} = 0, \quad \gamma_{23} = \frac{\partial u_2}{\partial x_3} + \frac{\partial u_3}{\partial x_2} = 0, \tag{7.5}$$

$$\gamma_{12} = \frac{\partial u_1}{\partial x_2} + \frac{\partial u_2}{\partial x_1} = -x_3\,\kappa_1(x_1), \quad \gamma_{13} = \frac{\partial u_1}{\partial x_3} + \frac{\partial u_3}{\partial x_1} = x_2\,\kappa_1(x_1), \tag{7.6}$$

where the *sectional twist rate* is defined as

$$\kappa_1(x_1) = \frac{\mathrm{d}\Phi_1}{\mathrm{d}x_1}. \tag{7.7}$$

The sectional twist rate, κ_1, measures the deformation of the circular cylinder. Note that a constant twist angle implies a rigid body rotation of the cylinder about its axis, but no deformation.

The axial strain field, eq. (7.4), vanishes because the section does not warp out-of-plane, and the in-plane strain field, eq. (7.5), vanishes because the in-plane motion of the section is a rigid body rotation. Under torsion, the only non-vanishing strain components are the out-of-plane shearing strains given by eq. (7.6).

This strain field is not easily visualized in rectangular coordinates because the Cartesian strain components, γ_{12} and γ_{13}, act in planes $(\bar{\imath}_1, \bar{\imath}_2)$ and $(\bar{\imath}_1, \bar{\imath}_3)$, respectively. In view of the cylindrical symmetry of the problem at hand, it is more natural to describe this strain field in the polar coordinate system, (r, α), shown in fig. 7.3. In this axis system, the corresponding strain components are γ_{r1} and $\gamma_{\alpha 1}$, where the second index refers to axis $\bar{\imath}_1$. For simplicity, however, these strain components will be simply denoted γ_α and γ_r.

The relationship between the Cartesian and polar strain components can be expressed using eq. (1.81) for a rotation, α, about axis $\bar{\imath}_1$, so that $\bar{\imath}_1^* = \bar{\imath}_1$, $\bar{\imath}_2^* = \bar{\imath}_r$, and $\bar{\imath}_3^* = \bar{\imath}_\alpha$. In this case, $\ell_1 = 1$, $\ell_2 = \ell_3 = 0$ and $m_1 = 0$, $m_2 = \cos\alpha$, $m_3 = \sin\alpha$ and $n_1 = 0$, $n_2 = -\sin\alpha$, $n_3 = \cos\alpha$. Using these direction cosines, eq. (1.81) then yields

$$\gamma_r = \gamma_{12}\cos\alpha + \gamma_{13}\sin\alpha, \quad \gamma_\alpha = -\gamma_{12}\sin\alpha + \gamma_{13}\cos\alpha. \tag{7.8}$$

Introducing the Cartesian shear strain components, eqs. (7.6), leads to

$$\gamma_r(x_1, r, \alpha) = 0, \quad \gamma_\alpha(x_1, r, \alpha) = r\,\kappa_1(x_1). \tag{7.9}$$

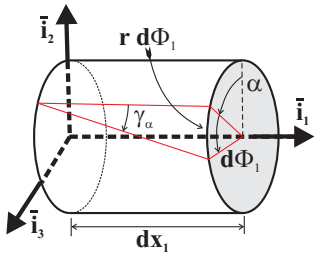

Fig. 7.4. Visualization of out-of-plane shear strain in polar coordinates.

The only non-vanishing strain component is the circumferential shearing strain component, γ_α, which is proportional to the twist rate, κ_1, and varies linearly from zero at the center of the section to its maximum value, $R\kappa_1$, along the outer edge of the cylinder. It is of course independent of circumferential variable α, as required by the cylindrical symmetry of the problem.

This strain component is depicted in fig. 7.4. Each circular cross-section retains its circular shape and experiences no in-plane or out-of-plane deformation: two adjacent sections experience a small differential rotation, $\mathrm{d}\Phi_1$, which gives rise to the circumferential shearing strain γ_α. As illustrated in fig. 7.4, the shearing strain is readily obtained as $\gamma_\alpha = r\,\mathrm{d}\Phi_1/\mathrm{d}x_1 = r\kappa_1$, in agreement with eq. (7.9).

7.1.2 The stress field

Let the cylinder be made of a linearly elastic material that obeys Hooke's law, eq. (2.9). In view of the strain field, eq. (7.6), the only non-vanishing stress components are

$$\tau_{12} = -Gx_3\,\kappa_1(x_1), \quad \tau_{13} = Gx_2\,\kappa_1(x_1), \tag{7.10}$$

where G is the shear modulus of the material. Once again, polar coordinates are more convenient to use in visualizing the stress field, which is obtained from eq. (7.9) and Hooke's law as

$$\tau_r(x_1, r, \alpha) = 0, \quad \tau_\alpha(x_1, r, \alpha) = Gr\ \kappa_1(x_1), \tag{7.11}$$

where τ_r and τ_α are the radial and circumferential shear stress components, respectively.

The distribution of the circumferential shear stress over the cross-section is shown in fig. 7.5. Two characteristics of this distribution should be noted. First, at all points, the shear stress acts in the circumferential direction, and the component in the radial direction vanishes. Second, the magnitude of the stress varies linearly along the radial direction: it is zero at the center and maximum at the largest radius. This implies that the central region of the bar does not experience very high stress values and is not very effective in resisting torsion. The peak stresses is reached at the outer radius of the bar.

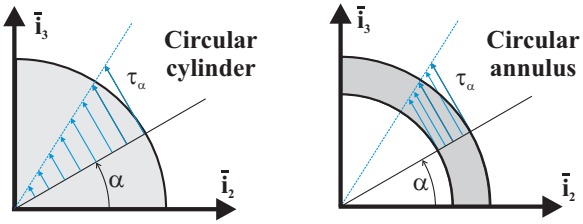

Fig. 7.5. Distribution of circumferential shearing stress over the cross-section.

7.1.3 Sectional constitutive law

The torque acting on the cross-section at a given span-wise location is readily obtained by integrating the circumferential shear stress, τ_α, multiplied by the moment arm, r, over the circular cross-section to find

$$M_1(x_1) = \int_{\mathcal{A}} \tau_\alpha r \, \mathrm{d}\mathcal{A}. \tag{7.12}$$

Introducing the circumferential shear stress, eq. (7.11) then yields

$$M_1(x_1) = \int_{\mathcal{A}} Gr^2 \kappa_1(x_1) \, \mathrm{d}\mathcal{A} = \left[\int_{\mathcal{A}} Gr^2 \, \mathrm{d}\mathcal{A}\right] \kappa_1(x_1) = H_{11}\ \kappa_1(x_1), \tag{7.13}$$

where the *torsional stiffness* of the section is defined as

$$H_{11} = \int_{\mathcal{A}} Gr^2 \, \mathrm{d}\mathcal{A}. \tag{7.14}$$

Relationship (7.13) is the constitutive law for the torsional behavior of the beam. It expresses the proportionality between the torque and the twist rate, with a constant of proportionality, H_{11}, called the torsional stiffness. Formula (7.14) is true *for circular cross-sections only*.

If the section is made of a homogeneous material of shear modulus G, the torsional stiffness then becomes $H_{11} = GJ$, where $J = \int_{\mathcal{A}} r^2 \, \mathrm{d}\mathcal{A}$ is the purely geometric integral known as the area polar moment. The entire theory is developed for bars with circular cross-sections, and therefore this expression for the torsional stiffness is valid *for circular cross-sections only*.

7.1.4 Equilibrium equations

The equations of equilibrium associated with the torsional behavior can be obtained by considering the infinitesimal slice of the cylinder of length $\mathrm{d}x_1$ depicted in fig. 7.6. Using a Taylor series expansion, the moment acting on the right-hand face is $M_1(x_1 + \mathrm{d}x_1) = M_1(x_1) + (\mathrm{d}M_1/\mathrm{d}x_1)\mathrm{d}x_1$, where higher order differential terms have been neglected. Summing all the moments acting about axis $\bar{\imath}_1$ then yields the torsional equilibrium equation

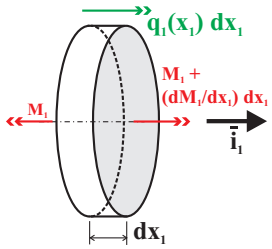

Fig. 7.6. Torsional loads acting on an infinitesimal slice of the bar.

$$\frac{\mathrm{d}M_1}{\mathrm{d}x_1} = -q_1. \tag{7.15}$$

7.1.5 Governing equations

Finally, the governing equation for the torsional behavior of circular cylinders is obtained by introducing the torque, eq. (7.13), into the equilibrium condition, eq. (7.15) and recalling the definition of the twist rate, eq. (7.7), to find

$$\frac{\mathrm{d}}{\mathrm{d}x_1}\left[H_{11}\,\frac{\mathrm{d}\Phi_1}{\mathrm{d}x_1}\right] = -q_1. \tag{7.16}$$

This second order differential equation can be solved for the twist distribution, $\Phi_1(x_1)$, given the applied torque distribution, $q_1(x_1)$.

Two boundary conditions involving the rotation, Φ_1, or the twist rate, κ_1, are required for the solution of eq. (7.16), one at each end of the cylinder. Typical boundary conditions are as follows.

1. A fixed (or clamped) end allows no rotation, *i.e.*, $\Phi_1 = 0$.
2. A free (unloaded) end corresponds to $M_1 = 0$, which, for eq. (7.13), can be expressed as $\kappa_1 = \mathrm{d}\Phi_1/\mathrm{d}x_1 = 0$.
3. Finally, if the end of the cylinder is subjected to a concentrated torque, Q_1, the boundary condition is $M_1 = Q_1$, which becomes $H_{11}\,\mathrm{d}\Phi_1/\mathrm{d}x_1 = Q_1$.

7.1.6 The torsional stiffness

The torsional stiffness of the section, H_{11}, characterizes the stiffness of the cylinder when subjected to torsion. If the cylinder is made of a homogeneous material, the shear modulus is identical at all points of the cross-section and can be factored out of eq. (7.14), which is then easily evaluated in polar coordinates

$$H_{11} = G \int_0^{2\pi} \int_0^R r^2 \, r \mathrm{d}r \mathrm{d}\alpha = \frac{\pi}{2} G R^4. \tag{7.17}$$

For a circular tube the second integral extends from the inner radius, R_i, to the outer radius, R_o, to find

$$H_{11} = G \int_0^{2\pi} \int_{R_i}^{R_o} r^2 \, r \mathrm{d}r \mathrm{d}\alpha = \frac{\pi}{2} G (R_o^4 - R_i^4). \tag{7.18}$$

A common situation of great practical importance is that of a thin-walled circular tube. Let the mean radius of the tube be $R_m = (R_o + R_i)/2$, and the wall thickness $t = R_o - R_i$. The thin wall assumption implies $t/R_m \ll 1$. The torsional stiffness of the thin-walled tube then becomes

$$H_{11} = \frac{\pi}{2} G (R_o^2 + R_i^2)(R_o + R_i)(R_o - R_i) \approx 2\pi G R_m^3 t. \tag{7.19}$$

Consider now a thin-walled circular tube consisting of N concentric layers of different materials through the thickness of the wall, as depicted in fig. 7.7. Assuming the material to be homogeneous within each layer, the torsional stiffness becomes

$$H_{11} = \frac{\pi}{2} \sum_{i=1}^{N} G^{[i]} \left[(R^{[i+1]})^4 - (R^{[i]})^4 \right],$$

where $G^{[i]}$ is the shear modulus in layer i. For a thin-walled tube, each layer will be thin, and the above approximation can be used once again to find

$$H_{11} = 2\pi \sum_{i=1}^{N} G^{[i]} t^{[i]} \left(\frac{R^{[i+1]} + R^{[i]}}{2} \right)^3. \tag{7.20}$$

The torsional stiffness is the *weighted average* of the shear moduli of the various layers. The weighting factor, $t^{[i]} \left[(R^{[i+1]} + R^{[i]})/2 \right]^3$, strongly biases the average in favor of the outermost layers.

7.1.7 Measuring the torsional stiffness

In the previous section, the torsional stiffness of a circular cylinder is computed from the geometry of the cross-section and the properties of the constituent materials. For example, eq. (7.17) gives the torsional stiffness for a cylinder made of a homogeneous, isotropic material, while eq. (7.20) gives the stiffness for a thin-walled tube

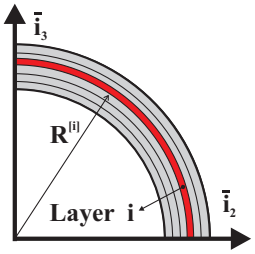

Fig. 7.7. Thin-walled tube made of layered materials.

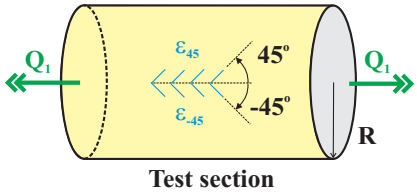

Fig. 7.8. Configuration of the test to determine the torsional stiffness.

made of composite materials. It is possible to experimentally measure the torsional stiffness of a cylinder using the torsional test set-up depicted in fig. 7.8. The torque, Q_1, is applied to the test sample by a torsional testing machine.

The deformation of the test section can be measured by the chevron strain gauge shown in fig. 1.24. Two strain gauges oriented at ± 45 degree angles with respect to the axis of the cylinder, as shown in fig. 7.8, yield the shear strain at the outer surface of the cylinder. In view of eq. (1.102), $\gamma_{12} = e_{+45} - e_{-45}$, where e_{+45} and e_{-45} are the extensional strain measurements along these two directions. Using eq. (7.9), this shear strain can be related to the twist rate of the cylinder: $\gamma_{12} = \gamma_\alpha = R\kappa_1$, where R is the radius of the cylinder. It then follows that $\kappa_1 = (e_{45} - e_{-45})/R$.

The test procedure is as follows. The circular cylinder is placed in the torsional testing machine and a torque Q_1 of increasing magnitude is applied. For each loading level, the corresponding deformation is measured by the strain gauges. The raw test data consists of loading levels, Q_{1i}, $i = 1, 2, \ldots, n$, where n is the number of data points, and the corresponding strains, ϵ_{45i} and e_{-45i}. From this raw data, the deformation of the cylinder is computed, $\kappa_{1i} = (e_{45i} - e_{-45i})/R$. This computed data is then plotted in the following manner: deformation, κ_{1i}, along the abscissa and torque, Q_{1i}, along the ordinate.

If the applied load remains small, the behavior of the cylinder is expected to be linear as expressed by eq. (7.13), *i.e.*, a linear relationship should be observed between torque and twist rate. Hence, the slope of the experimentally obtained Q_{3i} versus κ_{1i} curve should yield the torsional stiffness of the cylinder. Note that this experimental technique is valid for cylinders made of homogeneous materials, or for complex constructions involving many layers of concentric composite materials, as long as the cylindrical symmetry of the sample is maintained.

7.1.8 The shear stress distribution

The local circumferential shear stress can be related to the sectional torque by eliminating the twist rate between eqs. (7.11) and (7.13) to find

$$\tau_\alpha = G\frac{M_1(x_1)}{H_{11}}\, r. \tag{7.21}$$

where G is the shear modulus at the location where the stress is computed.

The shear strain defined by eq. (7.9) increases linearly from zero at the center of the circular section to a maximum value at the outer radius. As discussed in section 7.1, this linear distribution of shear strain is a direct consequence of the symmetries of the problem, and is independent of the bar's constituent materials. If the bar is made of a homogeneous material, the linear distribution of shear strains results in a linear distribution of shear stresses, as implied by eq. (7.21) and depicted in fig. 7.5. On the other hand, if the section is made of concentric layers of distinct material as depicted in fig. 7.7, the shear stress in layer i, denoted $\tau_\alpha^{[i]}$, is still given by eq. (7.21) as $\tau_\alpha^{[i]} = G^{[i]}(M_1/H_{11})\ r$. Within each layer, the shear stress distribution is still linear, but discontinuities might appear at the interface between the various layers.

The maximum shear stress in a section of homogeneous material occurs at the largest value of r, *i.e.*, at the outer edge of the cylinder. For a circular cylinder, the torsional stiffness is given eq. (7.17) and the magnitude of maximum shear stress becomes

$$\tau_\alpha^{\max} = \frac{2M_1(x_1)}{\pi R^3}. \tag{7.22}$$

For a circular tube, the torsional stiffness is given eq. (7.18), and the magnitude of maximum shear stress is

$$\tau_\alpha^{\max} = \frac{2R_o M_1(x_1)}{\pi(R_o^4 - R_i^4)}. \tag{7.23}$$

Finally, for a thin-walled circular tube, the shear stress distribution becomes nearly uniform through-the-thickness of the wall,

$$\tau_\alpha^{\max} \approx \frac{M_1(x_1)}{2\pi R_m^2 t}. \tag{7.24}$$

Similarly, the shear stress distribution in a tube made of thin concentric layers of various materials will be nearly uniform within each layer

$$\tau_\alpha^{[i]} \approx G^{[i]} \frac{R^{[i+1]} + R^{[i]}}{2} \frac{M_1(x_1)}{H_{11}}, \tag{7.25}$$

where the torsional stiffness, H_{11}, is given by eq. (7.20).

Once the local shear stress is determined, a strength criterion is applied to determine whether the structure can sustain the applied loads. For a cylindrical bar, combining the strength criterion, eq. (2.28) and the shear stress distribution given by eq. (7.21) yields $GR|M_1(x_1)|/H_{11} \leq \tau_{\text{allow}}$, where τ_{allow} is the allowable shear stress for the material. Since the torque varies along the bar's span, this condition must be checked at all points along the span. In practice, it is convenient to first determine the maximum torque, denoted $M_1^{\max}$, then apply the strength criterion

$$\frac{GR}{H_{11}}|M_1^{\max}| \leq \tau_{\text{allow}}. \tag{7.26}$$

If the section consists of layers made of various materials, the strength of each layer will, in general, be different, and the strength criterion becomes

$$\frac{G^{[i]}R^{[i+1]}}{H_{11}}|M_1^{\max}| \leq \tau_{\text{allow}}^{[i]}, \tag{7.27}$$

where $\tau_{\text{allow}}^{[i]}$ is the allowable shear stresses for layer i. The strength criterion must be checked for each material layer.

7.1.9 Rational design of cylinders under torsion

The shear stress distribution in a cylinder subjected to torsion is shown in fig. 7.5. Clearly, the material near the center of the cylinder is not used efficiently because the shear stress becomes small in the central portion of the cylinder. A far more efficient design is the thin-walled tube. Indeed, the shear stress becomes nearly uniform through-the-thickness of the wall, and all the material is used at full capacity.

For a homogeneous, thin-walled tube, the mass of material per unit span is $\mu = 2\pi R_m t\rho$, where ρ is the material density, R_m the mean radius, and t the thickness. The torsional stiffness, eq. (7.19), now becomes

$$H_{11} = 2\pi G R_m^3 t = \frac{\mu}{\rho} G R_m^2.$$

Consider two thin-walled tubes made of identical materials, with identical masses per unit span, but with mean radii, R_m and R'_m, respectively, and thicknesses t and t', respectively. Because the mass per unit span are equal, the thicknesses of the two tubes will be in inverse proportion of their radii, $t/t' = R'_m/R_m$. The ratio of their torsional stiffnesses, denoted H_{11} and H'_{11}, respectively, is

$$\frac{H_{11}}{H'_{11}} = \frac{(\mu/\rho)GR_m^2}{(\mu/\rho)GR'^2_m} = \left(\frac{R_m}{R'_m}\right)^2. \tag{7.28}$$

For two tubes of equal mass, the torsional stiffness increases with the square of the mean radius.

When subjected to identical torques, the ratio of the shear stresses in the two tubes, denoted τ_α and τ'_α, respectively, becomes

$$\frac{\tau_\alpha}{\tau'_\alpha} = \frac{GM_1R_m/H_{11}}{GM_1R'_m/H'_{11}} = \frac{R_mH'_{11}}{R'_mH_{11}} = \frac{R'_m}{R_m}. \tag{7.29}$$

For two tubes of equal mass, the shear stress is inversely proportional to the mean radius.

The ideal structure to carry torsional loads is a thin-walled tube with a large mean radius, because this yields the highest torsional stiffness and lowest maximum shear stress for a given mass of material and applied torque. In specific applications, limits will be placed on how large the mean radius can be. Furthermore, very thin-walled tubes can become unstable through a phenomenon called *torsional buckling*. This type of instability puts a limit on how thin the wall can be.

7.1.10 Problems

Problem 7.1. Torsion of a bimetallic bar
A circular bar is constructed by bonding an aluminum shell around a solid steel cylinder. The radius of the steel cylinder is $R_S = 10$ mm, and the outer radius of the aluminum shell is $R_A = 20$ mm. The overall length of the bar is given by $L = 1$ m, and a torque $T = 1$ kN·m is applied at the ends. The shear moduli for the aluminum and steel are $G_A = 28$ GPa and $G_S = 76$ GPa, respectively. *(1)* Find the maximum shear stress in the steel and in the aluminum. *(2)* Determine the total twist angle of the bar. *(3)* Determine the torsional stiffness. *(4)* Find the allowable torque for a safety factor of 2 when the yield stresses for both materials is 300 MPa.

Problem 7.2. Torsion of a circular bar with hollow segment
The cylindrical bar shown in fig. 7.9 consists of two segments; the left segment is clamped at point **R**, $\Phi_1(0) = 0$. The left segment of length L is a solid circular bar of radius R_O, while the right segment of length L is a hollow circular bar of inner radius R_i. A moment Q_1 is applied at point **T**. *(1)* Determine the twist angle at point **T**. *(2)* Determine the equivalent torsional stiffness, H, for the complete bar, defined as $H = \Phi_1(2L)/Q_1$. *(3)* Determine ratio of maximum shear stress in the two sections.

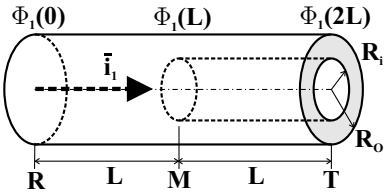

Fig. 7.9. Circular bar with hollow segment.

Problem 7.3. Torsion of a circular bar with hollow segment
The cylindrical bar shown in fig. 7.9 consists of two segments, clamped at point **R** and **T**, $\Phi_1(0) = \Phi_1(2L) = 0$. The left segment of length L is a solid circular bar of radius R_O, while the right segment of length L is a hollow circular bar of inner radius R_i. A moment Q_1 is applied at point **M**. *(1)* Determine the torque carried in each segment. *(2)* Determine the twist angle at point **M**. *(3)* Determine the equivalent torsional stiffness, H, at point **M**, defined as $H = \Phi_1(L)/Q_1$. *(4)* Determine the maximum shear stress in each segment.

Problem 7.4. Torsion of a hollow bar
A circular bar of radius $R = 200$ mm is replaced by a hollow bar of inner and outer radii R_i and R_o, respectively, with $R_0/R_i = 2$. If the two bars are made of the same material and can carry the same maximum torque, determine *(1)* the outer radius of the hollow bar, R_o, and *(2)* the mass ratio for the hollow and solid bars.

7.2 Torsion combined with axial force and bending moments

An aircraft propeller is connected to a homogeneous, circular shaft. The engine applies a torque to the shaft resulting in the shear stress distribution described in section 7.1.8. On the other hand, the propeller creates a thrust that generates a uniform

axial stress distribution over the cross-section. If the torque acts alone, the yield criterion is $\tau < \tau_y$. If the axial force acts alone, the corresponding criterion is $\sigma < \sigma_y$. The question is now: what is the proper strength criterion to be used when both axial and shear stresses are acting simultaneously? The yield criteria developed in section 2.3 will be used to answer this question.

Propeller shaft under torsion and thrust

Consider an aircraft propeller connected to a homogeneous, circular shaft of radius R. The engine applies a torque M_1 to the shaft and the propeller exerts a thrust N_1; the corresponding stresses are

$$\tau = \frac{2M_1}{\pi R^3}, \text{ and } \quad \sigma = \frac{N_1}{\pi R^2}. \tag{7.30}$$

Clearly, the shaft is in a state of plane stress, and Tresca's criterion, eq. (2.31), requires the following inequalities to hold

$$\left| \frac{1}{2}\frac{N_1}{\pi R^2} \pm \sqrt{\frac{1}{4}\left(\frac{N_1}{\pi R^2}\right)^2 + 4\left(\frac{M_1}{\pi R^3}\right)^2} \right| \leq \sigma_y,$$

$$2\sqrt{\frac{1}{4}\left(\frac{N_1}{\pi R^2}\right)^2 + 4\left(\frac{M_1}{\pi R^3}\right)^2} \leq \sigma_y.$$

if the material is to be free of yielding. Of these three conditions, the last is the most stringent, and hence, Tresca's yield criterion corresponds to an ellipse,

$$\left(\frac{N_1}{\pi R^2 \sigma_y}\right)^2 + 16\left(\frac{M_1}{\pi R^3 \sigma_y}\right)^2 = 1.$$

Figure 7.10 shows the geometric interpretation of the criterion. The structure behaves in a linearly elastic manner under combined loadings represented by points inside an ellipse drawn in the non-dimensional load space. The non-dimensional torque is $M_1/(\pi R^3 \sigma_y)$ and the non-dimensional axial force is $N_1/(\pi R^2 \sigma_y)$.

If the von Mises criterion, eq. (2.36), is applied instead, the material will behave in a linearly elastic manner when the following condition is satisfied

$$\left[\left(\frac{N_1}{\pi R^2}\right)^2 + 3\left(\frac{2M_1}{\pi R^3}\right)^2\right]^{1/2} \leq \sigma_y.$$

Here again, the criterion is conveniently recast into a non-dimensional form as

$$\left(\frac{N_1}{\pi R^2 \sigma_y}\right)^2 + 12\left(\frac{M_1}{\pi R^3 \sigma_y}\right)^2 \leq 1.$$

where the terms in parentheses are non-dimensional loading components defined earlier. Figure 7.10 shows this ellipse in the non-dimensional loading space. As expected, the predictions of Tresca's and von Mises' criteria differ most when the loading primarily generates shear stresses, *i.e.*, along the applied torque axis, see section 2.3.3.

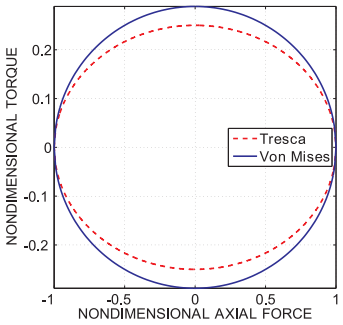

Fig. 7.10. Yield envelopes predicted by Tresca's and von Mises' criteria plotted in the non-dimensional loading space.

Shaft under torsion and bending

Consider now a circular shaft subjected to both bending and torsion, as would occur, for instance, in a cantilever shaft with a loaded tip pulley. Let M_3 and M_1 be the applied bending moment and torque, respectively. The corresponding axial and shear stress components are

$$\sigma = \frac{4M_3 r}{\pi R^4}, \text{ and } \quad \tau = \frac{2M_1 r}{\pi R^4}, \tag{7.31}$$

respectively. The maximum values occur at the same location on the cross-section at the upper or lower edge where $\sigma = 4M_3/\pi R^3$ and $\tau = 2M_1/\pi R^3$. Clearly, the shaft is in a state of plane stress, and Tresca's criterion, eq. (2.31), requires the following inequalities to hold

$$\left| \frac{2M_3}{\pi R^3} \pm \sqrt{\left(\frac{2M_3}{\pi R^3}\right)^2 + 4\left(\frac{M_1}{\pi R^3}\right)^2} \right| \leq \sigma_y,$$

$$2\sqrt{\left(\frac{2M_3}{\pi R^3}\right)^2 + 4\left(\frac{M_1}{\pi R^3}\right)^2} \leq \sigma_y,$$

if the material is to be free of yielding. Of these three conditions, the last is the most stringent, and hence, Tresca's yield criterion corresponds to an ellipse

$$16\left(\frac{M_3}{\pi R^3 \sigma_y}\right)^2 + 16\left(\frac{M_1}{\pi R^3 \sigma_y}\right)^2 = 1.$$

Figure 7.11 shows the geometric interpretation of the criterion. The structure behaves in a linearly elastic manner for combined loadings represented by points inside an ellipse drawn in the non-dimensional loading space defined by non-dimensional torque, $M_1/(\pi R^3 \sigma_y)$, and non-dimensional bending moment, $M_3/(\pi R^3 \sigma_y)$.

If von Mises' criterion, eq. (2.36), is applied instead, the material will behave in a linearly elastic manner when the following condition is satisfied

$$\left[\left(\frac{4M_3}{\pi R^2}\right)^2 + 3\left(\frac{2M_1}{\pi R^3}\right)^2\right]^{1/2} \leq \sigma_y$$

Here again, the criterion is conveniently recast into a non-dimensional form as

$$16\left(\frac{M_3}{\pi R^3 \sigma_y}\right)^2 + 12\left(\frac{M_1}{\pi R^3 \sigma_y}\right)^2 \leq 1,$$

Figure 7.11 shows this ellipse in the non-dimensional loading space.

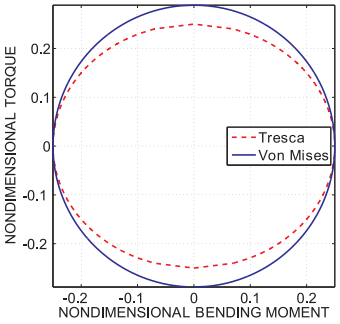

Fig. 7.11. Yield envelopes predicted by Tresca's and von Mises' criteria plotted in the non-dimensional loading space.

7.2.1 Problems

Problem 7.5. Pressure vessel subjected to combined loading
Consider the pressure vessel subjected to an internal pressure p_i and an external torque Q, as depicted in fig. 7.12. The pressure vessel is of radius R and wall thickness t. Use von Mises criterion to compute the failure envelope in the non-dimensional loading space defined by $Q/(tR^2\sigma_{\text{allow}})$ and $p_i R/(t\sigma_{\text{allow}})$.

Problem 7.6. Pressure vessel subjected to combined loading
The experimental set-up depicted in fig. 7.13 is aimed at studying the behavior of materials under complex stress states. A thin-walled pressure vessel of radius $R = 11$ mm and thickness $t = 2.0$ mm is subjected to an internal pressure p_i. At the same time, a normal force, N, and a torque, Q, are applied to the sample. In a specific experiment, the applied normal force is $N = 16$ kN and the internal pressure $p_i = 20$ MPa. The applied torque is slowly increased. The first permanent deformations are observed at the outer surface of the sample when $Q = 120$ N·m.
(1) Find the yield stress for the material if it is assumed to follow von Mises' yield criterion.
(2) Find the yield stress for the material if it is assumed to follow Tresca's yield criterion.
(3) Find and plot the yield surface in the space defined by the three loading components, the internal pressure, the applied axial force, and the applied torque.

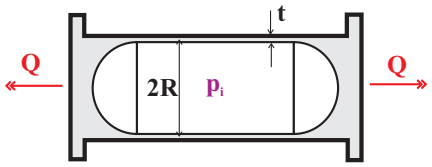

Fig. 7.12. Pressure vessel subjected to an external torque.

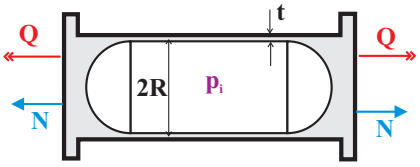

Fig. 7.13. Pressure vessel subjected to internal pressure, external torque and axial force.

Problem 7.7. Beam with circular section under bending and torsion
Consider a cantilevered beam of length $L = 1$ m with a circular cross-section of inner radius $R_i = 45$ mm and outer radius $R_o = 50$ mm. The beam is subjected to a tip torque $Q = 7$ kN·m and a tip transverse load P. Find the maximum allowable transverse load $P_{\max}$ if the allowable stress for the material is $\sigma_{\text{allow}} = 450$ MPa. Note: for a hollow circular section, $H^c_{22} = H^c_{33} = \pi E(R_o^4 - R_i^4)/4$.

7.3 Torsion of bars with arbitrary cross-sections

The theory of torsion presented in the two previous sections is valid for *bars with circular cross-sections only*. In this section, the theory of torsion will be generalized to bars presenting cross-sections of arbitrary shape.

7.3.1 Introduction

When analyzing the torsional behavior of circular cylinders, the circular symmetry of the problem leads to the conclusion that each cross-section rotates about its own center like a rigid disk. If this type of deformation is assumed to remain valid for a bar of arbitrary cross-section, the displacement field, eqs. (7.2) and (7.3), and the corresponding strain field, eqs. (7.4) to (7.6), will also describe the kinematics of bars with arbitrary sections. The only remaining stress component are the circumferential shear stress given by eq. (7.11).

Unfortunately, this assumption can lead to grossly erroneous results because the solution it implies violates the equilibrium equations of the problem along the edge of the section. Consider, for instance, torsion of the rectangular bar depicted in fig. 7.14. The circumferential shear stress, τ_α, given by eq. (7.11), is shown at an edge of the section, and it is resolved into its Cartesian components, τ_{12} and τ_{13}. In view of the principle of reciprocity of shear stresses, eq. (1.5), the existence of a stress component, τ_{13}, acting on the cross-section of the bar implies the existence of a shear stress component of equal magnitude acting on the orthogonal face, which happens to be the outer surface of the bar. Since the outer surface of the bar is stress free, the shear stress component, τ_{13}, must vanish on both faces. Consequently, the only shear stress component that can exist along the edge is component, τ_{12}, which is parallel to the edge. This reasoning can be applied to any point along the edge of the section, and consequently, *at any point along the edge of the bar's section, the shear stress*

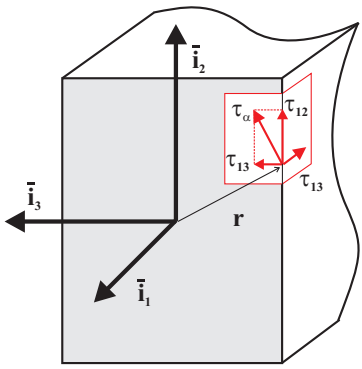

Fig. 7.14. Shearing stresses along the edge of a rectangular section.

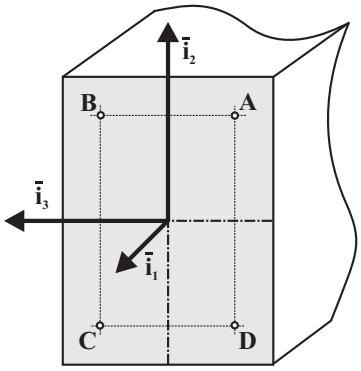

Fig. 7.15. Four points on a rectangular cross-section.

must be tangent to the edge. This condition is satisfied by the shear stress distribution acting on the circular section depicted in fig. 7.5, but the same circumferential shear stress distribution is not correct for the rectangular section shown in fig. 7.14.

As discussed in section 7.1, the symmetries associated with a circular cylinder imply that the bar's cross-section does not warp out-of-plane. No such conclusion can be reached for the rectangular section shown in fig. 7.15, because it presents fewer symmetries than the circular section. Indeed, the rectangular section is symmetric with respect to planes $(\bar{\imath}_1, \bar{\imath}_2)$ and $(\bar{\imath}_1, \bar{\imath}_3)$, but does not present the circular symmetry about axis $\bar{\imath}_1$ characteristic of a circular section. Since the section is symmetric with respect to plane $(\bar{\imath}_1, \bar{\imath}_2)$ but the torsional loading is antisymmetric with respect to the same plane, the solution must be antisymmetric with respect to this plane, *i.e.*, $u_1^A = -u_1^B$ and $u_1^C = -u_1^D$, where u_1^A, u_1^B, u_1^C and u_1^D, are the axial displacement components at points **A**, **B**, **C**, and **D**, respectively. Similarly, the antisymmetry of the solution with respect to plane $(\bar{\imath}_1, \bar{\imath}_3)$ implies $u_1^A = -u_1^D$ and $u_1^B = -u_1^C$. Combining the results then leads to $u_1^A = -u_1^B = u_1^C = -u_1^D$, which does not imply the vanishing of axial displacement at any of these points.

The same reasoning can be repeated for any set of four points symmetrically located with respect to the two planes of symmetry of the section. It follows that while the axial displacement field does present symmetries for the rectangular section, it does not vanish; in other words, *the section warps* out-of-plane. In general, *bars of arbitrary shaped cross-sections will warp*, in contrast with circular sections which do not.

7.3.2 Saint-Venant's solution

The solution to the problem of torsion of a bar with a cross-section of arbitrary shape was first given by Saint-Venant. The solution process provides a good application of basic elasticity theory and at the same time yields results of practical importance.

Kinematic description

Consider a solid bar with a cross-section of arbitrary shape. The area of the cross section is denoted $\mathcal{A}$, while its outer contour is defined by curve $\mathcal{C}$. The bar is of infinite length and is subjected to end torques. A closer look at the problem and experimental tests reveal that for a bar with an arbitrary section, each cross-section rotates like a rigid body, and warps out of its own plane. This type of deformation is described by the following assumed displacement field

$$u_1(x_1, x_2, x_3) = \Psi(x_2, x_3)\, \kappa_1(x_1), \tag{7.32a}$$

$$u_2(x_1, x_2, x_3) = -x_3 \Phi_1(x_1), \quad u_3(x_1, x_2, x_3) = x_2 \Phi_1(x_1). \tag{7.32b}$$

The in-plane displacement field, eq. (7.32b), describes a rigid body rotation of the cross-section, similar to the case for the circular cylinder, see eq. (7.3). The out-of-plane displacement field does not vanish, however. Instead, it is assumed to be proportional to the twist rate, κ_1, and has an arbitrary variation over the cross-section described by the unknown warping function, $\Psi(x_2, x_3)$. This warping function will be determined by enforcing equilibrium conditions for the resulting shear stress field. It will be further assumed that the twist rate is constant along the axis of the bar, *i.e.*, $\kappa_1(x_1) = \kappa_1$. This restriction results in what is known as the *uniform torsion* problem.

The strain field

Given the assumed displacement field defined by eqs. (7.32a) and (7.32b), the associated strain field can be evaluated based on the strain-displacement relationships, eqs. (1.63) and (1.71), to find

$$\varepsilon_1 = \Psi(x_2, x_3) \frac{\mathrm{d}\kappa_1}{\mathrm{d}x_1} = 0, \tag{7.33a}$$

$$\varepsilon_2 = 0, \quad \varepsilon_3 = 0, \quad \gamma_{23} = 0, \tag{7.33b}$$

$$\gamma_{12} = \left(\frac{\partial \Psi}{\partial x_2} - x_3 \right) \kappa_1, \quad \gamma_{13} = \left(\frac{\partial \Psi}{\partial x_3} + x_2 \right) \kappa_1. \tag{7.33c}$$

The vanishing of the axial strain, eq. (7.33a), is a direct consequence of the uniform torsion assumption, whereas the vanishing of the in-plane strains, eq. (7.33b) stems from the rigid body rotation assumption for the in-plane displacement field, eq. (7.32b). The only non-vanishing strain components, γ_{12} and γ_{13}, depend on the partial derivatives of the unknown warping function.

The stress field

For bars made of a linearly elastic, isotropic material, Hooke's law, eqs. (2.4) and (2.9), is assumed to apply. The stress field is then found from the strain field as

$$\sigma_1 = 0, \tag{7.34a}$$

$$\sigma_2 = 0, \quad \sigma_3 = 0, \quad \tau_{23} = 0, \tag{7.34b}$$

$$\tau_{12} = G\kappa_1 \left(\frac{\partial \Psi}{\partial x_2} - x_3 \right), \quad \tau_{13} = G\kappa_1 \left(\frac{\partial \Psi}{\partial x_3} + x_2 \right). \tag{7.34c}$$

Equilibrium equations

This stress field must satisfy the general equilibrium equations, eqs. (1.4), at all points of the section. Neglecting body forces, and in view of eq. (7.34b), two of the three equilibrium equations are identically satisfied and the remaining one reduces to

$$\frac{\partial \tau_{12}}{\partial x_2} + \frac{\partial \tau_{13}}{\partial x_3} = 0. \tag{7.35}$$

Introducing eqs. (7.34c), it follows that the warping function must satisfy the following partial differential equation

$$\frac{\partial^2 \Psi}{\partial x_2^2} + \frac{\partial^2 \Psi}{\partial x_3^2} = 0. \tag{7.36}$$

at all points of the cross-section.

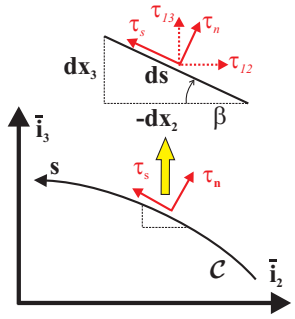

Fig. 7.16. Equilibrium condition along the outer contour $\mathcal{C}$.

The relevant boundary conditions can be developed by requiring the satisfaction of the equilibrium conditions along the outer edge of the section that defines curve $\mathcal{C}$. Figure 7.16 shows a portion of the outer contour, $\mathcal{C}$, and a curvilinear variable, s, that measures length along this curve.

As illustrated in fig. 7.14, the normal component of shear stress must vanish at all points along $\mathcal{C}$, *i.e.*,

$$\tau_n = 0, \tag{7.37}$$

whereas the component of shear stress, τ_s, tangent to the contour does not necessarily vanish. In terms of Cartesian components, the normal component of shear stress, see fig. 7.16, is

$$\tau_n = \tau_{12} \sin\beta + \tau_{13} \cos\beta = \tau_{12} \left(\frac{\mathrm{d}x_3}{\mathrm{d}s} \right) + \tau_{13} \left(-\frac{\mathrm{d}x_2}{\mathrm{d}s} \right) = 0. \tag{7.38}$$

Introducing eq. (7.34c) then yields the following boundary condition for the warping function

$$\left(\frac{\partial \Psi}{\partial x_2} - x_3 \right) \frac{\mathrm{d}x_3}{\mathrm{d}s} - \left(\frac{\partial \Psi}{\partial x_3} + x_2 \right) \frac{\mathrm{d}x_2}{\mathrm{d}s} = 0. \tag{7.39}$$

The warping function, $\Psi(x_2, x_3)$, is the solution of the following partial differential equation and associated boundary conditions,

$$\frac{\partial^2 \Psi}{\partial x_2^2} + \frac{\partial^2 \Psi}{\partial x_3^2} = 0, \text{ over } \mathcal{A}, \tag{7.40a}$$

$$\left(\frac{\partial \Psi}{\partial x_2} - x_3\right)\frac{\mathrm{d}x_3}{\mathrm{d}s} - \left(\frac{\partial \Psi}{\partial x_3} + x_2\right)\frac{\mathrm{d}x_2}{\mathrm{d}s} = 0, \text{ along } \mathcal{C}. \tag{7.40b}$$

This particular kind of partial differential equation is called *Laplace's equation*, and solution of this problem is rather complicated in view of the complex boundary condition that must hold along $\mathcal{C}$.

Prandtl's stress function

An alternative formulation of the problem that leads to simpler boundary conditions is found by introducing a *stress function*, ϕ, proposed by Prandtl. This function, $\phi(x_2, x_3)$, is defined as

$$\tau_{12} = \frac{\partial \phi}{\partial x_3}, \quad \tau_{13} = -\frac{\partial \phi}{\partial x_2}. \tag{7.41}$$

This shear stress field automatically satisfies the local equilibrium equation, as can be verified by introducing eq. (7.41) into eq. (7.35).

Next, the shear stresses, τ_{12} and τ_{13}, expressed in terms of the warping function by eq. (7.34c) must equal their counterparts expressed in terms of Prandtl's stress function by eq. (7.41) to find

$$\tau_{12} = G\kappa_1\left(\frac{\partial \Psi}{\partial x_2} - x_3\right) = \frac{\partial \phi}{\partial x_3}, \quad \tau_{13} = G\kappa_1\left(\frac{\partial \Psi}{\partial x_3} + x_2\right) = -\frac{\partial \phi}{\partial x_2}. \tag{7.42}$$

The warping function can be eliminated by taking a partial derivative of the first equation with respect to x_3 and a partial derivative of the second with respect to x_2. Subtracting these two equations then yields a single partial differential equation for Prandtl's stress function,

$$\frac{\partial^2 \phi}{\partial x_2^2} + \frac{\partial^2 \phi}{\partial x_3^2} = -2G\kappa_1. \tag{7.43}$$

The boundary conditions along $\mathcal{C}$ follow from eqs. (7.38) and (7.41)

$$\tau_n = \frac{\partial \phi}{\partial x_3}\frac{\mathrm{d}x_3}{\mathrm{d}s} + \frac{\partial \phi}{\partial x_2}\frac{\mathrm{d}x_2}{\mathrm{d}s} = \frac{\mathrm{d}\phi}{\mathrm{d}s} = 0. \tag{7.44}$$

which implies a constant value of ϕ along curve $\mathcal{C}$. If the section is bounded by several disconnected curves, the stress function must be a constant along each individual curve, although the value of the constant can be different for each curve. For solid cross-sections bounded by a single curve, the constant value of the stress function along that curve may be chosen to vanish because this choice has no effect on the resulting stress distribution.

The stress function is the solution of the following partial differential equation and associated boundary condition

$$\frac{\partial^2 \phi}{\partial x_2^2} + \frac{\partial^2 \phi}{\partial x_3^2} = -2G\kappa_1, \quad \text{on } \mathcal{A}, \tag{7.45a}$$

$$\frac{\mathrm{d}\phi}{\mathrm{d}s} = 0, \quad \text{along } \mathcal{C}. \tag{7.45b}$$

This partial differential equation is no longer homogeneous, a form referred to as *Poisson's equation*. The advantage of this formulation is that the boundary condition is much simpler than that obtained for the warping function, see eq. (7.40b).

Sectional equilibrium

The differential equations for the warping and stress functions are found from local equilibrium consideration. Global equilibrium of the section must also be verified. For a solid section bounded by a single contour, the resultant shear forces acting on the section are

$$V_2 = \int_{\mathcal{A}} \tau_{12} \, \mathrm{d}\mathcal{A} = \int_{x_2} \int_{x_3} \frac{\partial \phi}{\partial x_3} \, \mathrm{d}x_2 \mathrm{d}x_3 = \int_{x_2} \left[\int_{x_3} \frac{\partial \phi}{\partial x_3} \, \mathrm{d}x_3 \right] \, \mathrm{d}x_2 = 0,$$

and

$$V_3 = \int_{\mathcal{A}} \tau_{13} \, \mathrm{d}\mathcal{A} = \int_{x_2} \int_{x_3} -\frac{\partial \phi}{\partial x_2} \, \mathrm{d}x_2 \mathrm{d}x_3 = -\int_{x_3} \left[\int_{x_2} \frac{\partial \phi}{\partial x_2} \, \mathrm{d}x_2 \right] \, \mathrm{d}x_3 = 0,$$

where the last equalities follow from selecting a zero value for the stress function along the contour $\mathcal{C}$. This is the expected result because no shear forces are applied.

The total torque acting on the section is

$$M_1 = \int_{\mathcal{A}} (x_2 \tau_{13} - x_3 \tau_{12}) \, \mathrm{d}\mathcal{A} = \int_{\mathcal{A}} \left(-x_2 \frac{\partial \phi}{\partial x_2} - x_3 \frac{\partial \phi}{\partial x_3} \right) \, \mathrm{d}\mathcal{A}. \tag{7.46}$$

Integrating by parts then yields

$$M_1 = 2 \int_{\mathcal{A}} \phi \, \mathrm{d}\mathcal{A} - \int_{x_3} [x_2 \phi]_{x_2} \, \mathrm{d}x_3 - \int_{x_2} [x_3 \phi]_{x_3} \, \mathrm{d}x_2. \tag{7.47}$$

For solid cross-sections bounded by a single curve, the constant value of the stress function along that curve may be chosen as zero, and the boundary terms disappear, leading to the simple result

$$M_1 = 2 \int_{\mathcal{A}} \phi \, \mathrm{d}\mathcal{A}. \tag{7.48}$$

The applied torque equals twice the "volume" under the stress function. This formula applies only to solid cross-sections bounded by a single curve. Indeed, if the section is bounded by several disconnected curves, the stress function equals a different constant along each individual curve, and the boundary terms no longer vanish. For such

sections, the applied torque should be evaluated with the help of eq. (7.46) rather than (7.48).

In summary, the stress distribution in a bar of arbitrary cross-section subjected to uniform torsion can be obtained by evaluating either the warping or stress function from eqs. (7.40) or (7.45), respectively. The stress field then follows from eqs. (7.34c) or (7.41), respectively. Since all governing equations are satisfied, this represents an exact solution of the problem.

Saint-Venant's solution procedure is an example of the semi-inverse solution technique. The displacement field is assumed to be of the form given by eqs. (7.32). It is shown, however, that based on this displacement field, all equations of elasticity are satisfied, and hence the assumed displacement field must be the exact solution of the problem.

Example 7.1. Torsion of an elliptical bar

Consider a bar with an elliptical cross-section as shown in fig. 7.17. The equation for curve $\mathcal{C}$ defining the section is $(x_2/a)^2 + (x_3/b)^2 = 1$. A stress function of the following form is assumed

$$\phi = C_0 \left[\left(\frac{x_2}{a}\right)^2 + \left(\frac{x_3}{b}\right)^2 - 1 \right],$$

where C_0 is an unknown constant. The boundary condition, eq. (7.45b), is clearly satisfied since $\phi = 0$ along $\mathcal{C}$. Substituting this in the governing differential equation, eq. (7.45), leads to the following equation for constant C_0: $C_0(2/a^2 + 2/b^2) = -2G\kappa_1$, or $C_0 = -a^2b^2G\kappa_1/(a^2 + b^2)$. The stress function then becomes

$$\phi = -\frac{a^2b^2}{a^2 + b^2} \left[\left(\frac{x_2}{a}\right)^2 + \left(\frac{x_3}{b}\right)^2 - 1 \right] G\kappa_1. \tag{7.49}$$

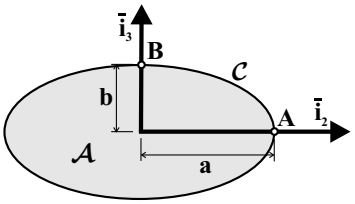

Fig. 7.17. A bar with an elliptical cross-section.

The torque can now be computed from eq. (7.48) to find

$$M_1 = -\frac{2a^2b^2}{a^2 + b^2} G\kappa_1 \int_{\mathcal{A}} \left[\left(\frac{x_2}{a}\right)^2 + \left(\frac{x_3}{b}\right)^2 - 1 \right] \mathrm{d}\mathcal{A} = G\frac{\pi a^3 b^3}{a^2 + b^2}\kappa_1 = H_{11}\kappa_1,$$

where $\int_{\mathcal{A}} \mathrm{d}\mathcal{A} = \pi ab$, $\int_{\mathcal{A}} x_2^2 \, \mathrm{d}\mathcal{A} = \pi a^3 b/4$, and $\int_{\mathcal{A}} x_3^2 \, \mathrm{d}\mathcal{A} = \pi ab^3/4$ are the ellipse's area and second moments of area about axes $\bar{\imath}_2$ and $\bar{\imath}_3$, respectively. The torsional stiffness of the elliptical section is

$$H_{11} = G\frac{\pi a^3 b^3}{a^2 + b^2}. \tag{7.50}$$

Using these results, the stress function can be expressed in terms of the applied torque

$$\phi = -\frac{M_1}{\pi ab}\left[\left(\frac{x_2}{a}\right)^2 + \left(\frac{x_3}{b}\right)^2 - 1\right].$$

The stress distribution then follows from eqs. (7.41),

$$\tau_{12} = -\frac{2x_3}{\pi ab^3}\, M_1, \quad \tau_{13} = \frac{2x_2}{\pi a^3 b}\, M_1.$$

The maximum shear stresses occur for the extreme values of x_2 and x_3, which are found along the section's boundary. The shear stress distributions along axes $\bar{\imath}_2$ and $\bar{\imath}_3$ are shown in fig. 7.18a: the maximum stresses are found points **B** and **A** as $\tau_{12}^B = -2M_1/(\pi ab^2)$ and $\tau_{13}^A = 2M_1/(\pi a^2 b)$, respectively. The maximum shear stress occurs at the end of the minor axis of the ellipse, *i.e.*, at point **B**, where

$$|\tau_{\max}| = \frac{2M_1}{\pi ab^2}.$$

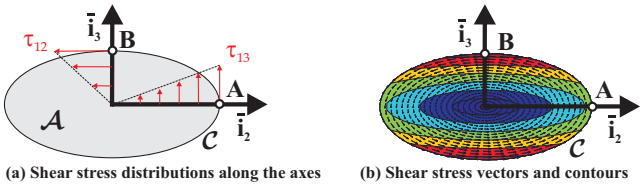

Fig. 7.18. Shear stress distribution for an elliptical cross-section.

Figure 7.18b shows the shear stress vectors over the cross-section; as required by the principle of reciprocity of shear stresses, eq. (1.5), the shear stress vectors along curve $\mathcal{C}$ are tangent to this curve.

Finally, the warping function can be obtained by integrating eq. (7.42). Substituting the calculated stress function, eq. (7.49), into these equations yields

$$\frac{\partial \Psi}{\partial x_2} = -\frac{a^2 - b^2}{a^2 + b^2} x_3, \quad \frac{\partial \Psi}{\partial x_3} = -\frac{a^2 - b^2}{a^2 + b^2} x_2.$$

Integrating the first equation with respect to x_2 and the second with respect to x_3 yields $\Psi = -x_2 x_3 (a^2 - b^2)/(a^2 + b^2) + f(x_3)$, and $\Psi = -x_2 x_3 (a^2 - b^2)/(a^2 + b^2) + g(x_2)$, respectively. These two solutions are equal only if $f(x_3) = g(x_2) = 0$, which implies $\Psi = -(a^2 - b^2)/(a^2 + b^2)\; x_2 x_3$. Equation (7.32a) now yields the warping displacement as

$$u_1(x_2, x_3) = -\kappa_1 \frac{a^2 - b^2}{a^2 + b^2}\, x_2 x_3. \tag{7.51}$$

Note that the elliptic cross-section presents two planes of symmetry, planes $(\bar{\imath}_1, \bar{\imath}_2)$ and $(\bar{\imath}_1, \bar{\imath}_3)$. As discussed in section 7.3.1, this implies that the warping displacement must be antisymmetric with respect to these two planes. The left portion of fig. 7.19 depicts the warping displacement with a contour plot immediately below it. A separate contour plot is shown in the right portion of the same figure. As expected for an antisymmetric function, the warping displacement vanishes along axes $\bar{\imath}_2$ and $\bar{\imath}_3$, and is of equal magnitude but opposite signs at points symmetrically located with respect to axes $\bar{\imath}_2$ and $\bar{\imath}_3$.

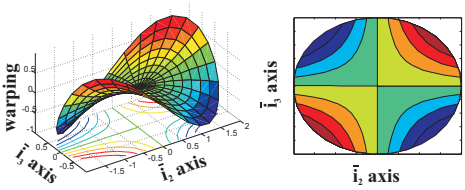

Fig. 7.19. Warping distribution for an elliptic cross-section.

For $a = b = R$, the bar with an elliptical section becomes a circular cylinder of radius R. The torsional stiffness for the elliptical section reduces to eq. (7.17), and the maximum shear stress to eq. (7.22). Finally, the warping function vanishes, and this is fully consistent with the symmetry arguments made for the circular cylinder proving that the warping displacement must vanish.

Example 7.2. Torsion of a thick cylinder

Consider a circular tube of inner radius R_i and outer radius R_o made of a homogeneous, isotropic material of shear modulus G, as shown in fig. 7.20. Note that this section is bounded by two curves, $\mathcal{C}_i$ and $\mathcal{C}_o$, as shown on the figure, that denote the inner and outer circles bounding the section.

The stress function for this problem is assumed to be in the following form: $\phi = Cr^2$, where $r^2 = x_2^2 + x_3^2$ and C is an unknown constant. The values of the stress function along curves $\mathcal{C}_i$ and $\mathcal{C}_o$ are $\phi_i = CR_i^2$ and $\phi_o = CR_o^2$, respectively. Since C, R_i and R_o are constants, this implies that the boundary conditions on the stress function, given by eq. (7.45b), are satisfied: $\mathrm{d}\phi_i/\mathrm{d}s_i = \mathrm{d}\phi_o/\mathrm{d}s_o = 0$, where s_i and s_o are curvilinear variables along $\mathcal{C}_i$ and $\mathcal{C}_o$, respectively. Note that the boundary condition requires ϕ to be *constant* along curves $\mathcal{C}_i$ and $\mathcal{C}_o$, but this does not imply that $\phi_i = 0$, or $\phi_o = 0$, or $\phi_i = \phi_o$.

Introducing the assumed stress function into the governing partial differential equation (7.45) yields $2C + 2C = -2G\kappa_1$. Hence, the stress function becomes $\phi = -G\kappa_1 r^2/2$. This represents the exact solution of the problem, because the stress function satisfies the governing partial differential equation and boundary conditions. The shear stress distribution then follows from eq. (7.41) as $\tau_{12} = -G\kappa_1 x_3$ and $\tau_{13} = G\kappa_1 x_2$. The torque generated by this shear stress distribution is evaluated with the help of eq. (7.46) to find

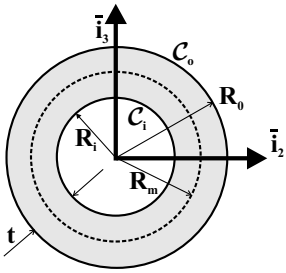

Fig. 7.20. Cross-section of a circular tube.

$$M_1 = \int_0^{2\pi} \int_{R_i}^{R_o} (x_2\tau_{13} - x_3\tau_{12})\ r\mathrm{d}r\mathrm{d}\alpha = \int_0^{2\pi} \int_{R_i}^{R_o} G\kappa_1(x_2^2 + x_3^2)\ r\mathrm{d}r\mathrm{d}\alpha$$
$$= \frac{\pi}{2} G\kappa_1(R_o^4 - R_i^4) = H_{11}\kappa_1,$$

where the Cartesian to polar coordinate transformation relationships, $x_2 = r\cos\alpha$ and $x_3 = r\sin\alpha$ are used. Using eq. (7.48) to evaluate the torque will yield incorrect results, as can be easily verified. This is because eq. (7.48) is derived assuming a *solid cross-section bounded by a single curve*; this is not the case for the present thick tube that is bounded by two curves, $\mathcal{C}_i$ and $\mathcal{C}_o$.

The torsional stiffness of the thick tube is $H_{11} = \pi G(R_o^4 - R_i^4)/2$, which matches the previously obtained result, eq. (7.18). It is left to the reader to show that the stress field obtained from the stress function matches that found in section 7.1.2.

7.3.3 Saint-Venant's solution for a rectangular cross-section

The formulation of the uniform torsion problem for bars of arbitrary cross-sectional shape is treated in section 7.3.2 and requires the solution of a partial differential equation for either the warping function, or the stress function, see eq. (7.40) or (7.45), respectively. Except for very simple geometries, such as the elliptical section treated in the previous example, the exact solution of the problem is arduous.

Two solutions of the uniform torsion problem for a rectangular cross-section are presented in this section. First, an approximate solution based on the co-location approach, then an exact solution based on Fourier series expansion.

Approximate solution

Consider a bar with a rectangular cross-section of width a and height b depicted in fig. 7.21. The following expression will be assumed for the stress function

$$\phi(\eta, \zeta) = C_0 \left(\eta^2 - \frac{1}{4}\right)\left(\zeta^2 - \frac{1}{4}\right),$$

where C_0 is an unknown constant, $\eta = x_2/a$ is the non-dimensional coordinate along axis $\bar{\imath}_2$, and $\zeta = x_3/b$ that along axis $\bar{\imath}_3$, as shown in fig. 7.21. This choice of

the stress function implies that $\phi(\eta = \pm 1/2, \zeta) = 0$ and $\phi(\eta, \zeta = \pm 1/2) = 0$, *i.e.*, ϕ vanishes along the edge, $\mathcal{C}$, of the section, as required by the boundary conditions of the problem, eq. (7.45b).

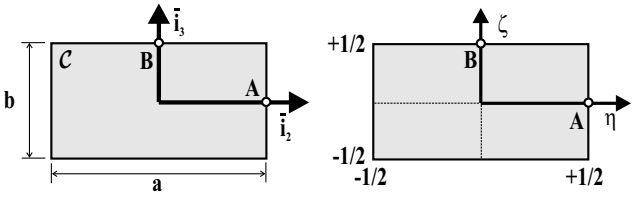

Fig. 7.21. Bar with a rectangular cross-section.

Using the chain rule for partial derivatives, $\partial/\partial x_2 = \partial/\partial\eta\ (\partial\eta/\partial x_2)$, where $\partial\eta/\partial x_2 = 1/a$; a similar expression holds for $\partial/\partial x_3$. Substituting the assumed stress function into the governing partial differential equation, eq. (7.43), then leads to $2C_0(\zeta^2 - 1/4)/a^2 + 2C_0(\eta^2 - 1/4)/b^2 = -2G\kappa_1$. This result shows that the assumed solution does not satisfy the partial differential equation.

A number of methods are available to construct approximate solutions, but one of the simplest is to satisfy this equation only a specific points of the cross-section, an approach called the *co-location method*. In this case, the governing partial differential equation will be satisfied at the center of the section, $(\eta, \zeta) = (0, 0)$, which implies $-C_0/(2a^2) - C_0/(2b^2) = -2G\kappa_1$. Solving for C_0 yields $C_0 = 4G\kappa_1 a^2 b^2/(a^2+b^2)$. The stress function now becomes

$$\phi(\eta, \zeta) = \frac{4a^2b^2G\kappa_1}{a^2 + b^2}\left(\eta^2 - \frac{1}{4}\right)\left(\zeta^2 - \frac{1}{4}\right).$$

For this section bounded by a single curve, the externally applied torque is given by eq. (7.48) as

$$M_1 = 2\int_{\mathcal{A}} \phi \, \mathrm{d}\mathcal{A} = \frac{a^2b^2G\kappa_1}{2(a^2 + b^2)} \int_{\mathcal{A}} \left(\eta^2 - \frac{1}{4}\right)\left(\zeta^2 - \frac{1}{4}\right) \mathrm{d}\mathcal{A} = \frac{2}{9}\frac{a^3b^3G\kappa_1}{a^2 + b^2}.$$

This result reveals the torsional stiffness, $H_{11} = M_1/\kappa_1$. The non-dimensional torsional stiffness, $\bar{H}_{11} = H_{11}/(ab^3G)$, then becomes

$$\bar{H}_{11} = \frac{H_{11}}{ab^3G} = \frac{2}{9}\frac{1}{1 + (b/a)^2}. \tag{7.52}$$

The stress function can be be expressed in terms of the applied torque as $\phi = 18M_1(\eta^2 - 1/4)(\zeta^2 - 1/4)/(ab)$. The shear stress field now follows from eqs. (7.41) as

$$\tau_{12} = \frac{1}{b}\frac{\partial\phi}{\partial\zeta} = \frac{36M_1}{ab^2}\left(\eta^2 - \frac{1}{4}\right)\zeta; \quad \tau_{13} = -\frac{1}{a}\frac{\partial\phi}{\partial\eta} = -\frac{36M_1}{a^2b}\eta\left(\zeta^2 - \frac{1}{4}\right).$$

Open form exact solution using a Fourier series

Consider once again the bar with a rectangular cross-section of width a and height b, as depicted in fig. 7.21. A Fourier series expansion of the stress function will be assumed as the solution of the problem,

$$\phi(\eta,\zeta) = \sum_{i=\text{odd}}^{\infty}\sum_{j=\text{odd}}^{\infty} C_{ij}\cos i\pi\eta\cos j\pi\zeta,$$

where $\eta = x_2/a$, $\zeta = x_3/b$, and C_{ij} are unknown coefficients.

First, it is verified that this assumed solution satisfies the boundary conditions of the problem, eq. (7.45b). Indeed, at $\eta = \pm 1/2$, $\cos(i\pi\eta) = \cos(\pm i\pi/2) = 0$ for all odd values of i; similarly, ϕ vanishes at $\zeta = \pm 1/2$ for all odd values of j. The function ϕ does not vanish along the boundaries for even values of i or j, and this is why only odd values of i and j are included in the expression for the stress function.

Substituting the above expression into the governing partial differential equation, eq. (7.43), yields

$$\sum_{i=\text{odd}}^{\infty}\sum_{j=\text{odd}}^{\infty} C_{ij}\left[\left(\frac{i\pi}{a}\right)^2 + \left(\frac{j\pi}{b}\right)^2\right]\cos i\pi\eta\cos j\pi\zeta = 2G\kappa_1.$$

This forms a set of equations for the unknown coefficients, C_{ij}. The evaluation of these coefficients relies on the orthogonality properties of cosine functions. The above equation is first multiplied by $\cos m\pi\eta\cos n\pi\zeta$, where m and n are arbitrary odd integers, then integrated over the cross-section to yield

$$\sum_{i=\text{odd}}^{\infty}\sum_{j=\text{odd}}^{\infty} C_{ij}\left[\left(\frac{i\pi}{a}\right)^2 + \left(\frac{j\pi}{b}\right)^2\right]\left[\int_{-1/2}^{1/2}\cos m\pi\eta\cos i\pi\eta\,\mathrm{d}\eta\right]$$
$$\left[\int_{-1/2}^{+1/2}\cos n\pi\zeta\cos j\pi\zeta\,\mathrm{d}\zeta\right] = -2G\kappa_1\left[\int_{-1/2}^{1/2}\cos m\pi\eta\,\mathrm{d}\eta\right]\left[\int_{-1/2}^{1/2}\cos n\pi\zeta\,\mathrm{d}\zeta\right].$$

The bracketed integrals can be evaluated in closed form with the help of eqs. (A.46b) and (A.47) and vanish when $m \neq i$ or $n \neq j$, thus eliminating the summations. The remaining terms are

$$C_{mn}\left[\left(\frac{m\pi}{a}\right)^2 + \left(\frac{n\pi}{b}\right)^2\right]\frac{1}{4} = \frac{8}{mn\pi^2}(-1)^{(m-1)/2}(-1)^{(n-1)/2}G\kappa_1.$$

Solving for the unknown coefficients, C_{mn}, then yields the stress function as

$$\phi(\eta,\zeta) = \frac{32G\kappa_1}{\pi^2}\sum_{i=\text{odd}}^{\infty}\sum_{j=\text{odd}}^{\infty}\frac{(-1)^{(i+j-2)/2}}{ij\left[(i\pi/a)^2 + (j\pi/b)^2\right]}\cos i\pi\eta\cos j\pi\zeta. \quad (7.53)$$

Since the section is bounded by a single curve, the externally applied torque is given by eq. (7.48)

$$M_1 = \frac{2^8}{\pi^6} ab^3 G\kappa_1 \sum_{i=\text{odd}}^{\infty} \sum_{j=\text{odd}}^{\infty} \frac{1}{(ij)^2 \left[i^2(b/a)^2 + j^2\right]} = H_{11}\kappa_1,$$

from which it follows that the non-dimensional torsional stiffness is

$$\bar{H}_{11} = \frac{H_{11}}{ab^3 G} = \frac{2^8}{\pi^6} \sum_{i=\text{odd}}^{\infty} \sum_{j=\text{odd}}^{\infty} \frac{1}{(ij)^2 \left[i^2(b/a)^2 + j^2\right]}. \tag{7.54}$$

Although in the form of a doubly infinite series, this expression for the torsional stiffness converges rapidly. For a bar with a square cross-section, $a = b$, the torsional stiffness obtained using the double sine series is $\bar{H}_{11} = 0.140577$. Considering only a single term in the series, $i = j = 1$, results in $\bar{H}_{11} = 2^8 \left[1/2\right] / \pi^6 = 0.133$, a 5% error. The four term series generated by i and j taking values of 1 and 3 yields $\bar{H}_{11} = 2^8 \left[1/2 + 1/90 + 1/90 + 1/1458\right] / \pi^6 = 0.139$, a 1% error.

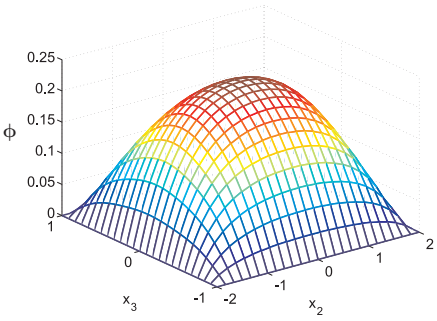

Fig. 7.22. Stress function, ϕ.

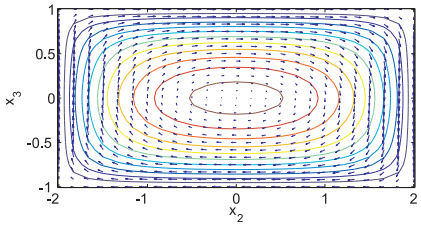

Fig. 7.23. Distribution of shear stress over cross-section. The arrows represent the shear stresses; the contours represent constant values of the stress function ϕ.

The shear stress field now follows from eqs. (7.41) as

$$\tau_{12} = -\frac{2^5}{\pi^3} \frac{bG}{H_{11}} M_1 \sum_{i=\text{odd}}^{\infty} \sum_{j=\text{odd}}^{\infty} \frac{(-1)^{(i+j-2)/2}}{i\left[i^2(b/a)^2 + j^2\right]} \cos\frac{i\pi x_2}{a} \sin\frac{j\pi x_3}{b}, \tag{7.55a}$$

$$\tau_{13} = \frac{2^5}{\pi^3} \frac{b^2 G}{aH_{11}} M_1 \sum_{i=\text{odd}}^{\infty} \sum_{j=\text{odd}}^{\infty} \frac{(-1)^{(i+j-2)/2}}{j\left[i^2(b/a)^2 + j^2\right]} \sin\frac{i\pi x_2}{a} \cos\frac{j\pi x_3}{b}. \tag{7.55b}$$

Here again, the results are in the form of a double sine series that is tedious to evaluate but converges rapidly. The stress function and shear stress distributions are shown in fig. 7.22 and 7.23, respectively, for $a = 4$ and $b = 2$. For the shear stress plot, the shear stress components, τ_{12} and τ_{13}, are converted into stress vectors and represented by arrows whose lengths are proportional to their magnitude.

Comparison of solutions

The Fourier series solution developed in the previous section converges to the exact solution to the problem as the number of terms used in the series increases. In

practice, nearly exact solutions can be obtained by using a large but finite number of terms in all series; this will be referred to as the exact solution. The solution obtained from the co-location approach will be referred to as the approximate solution.

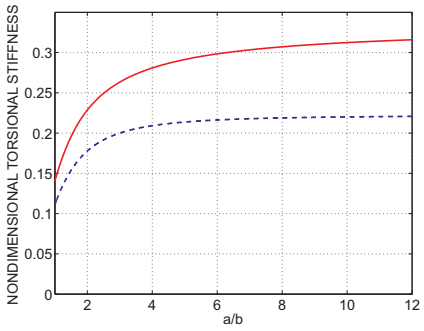

Fig. 7.24. Non-dimensional torsional stiffness, $\bar{H}_{11}$, versus aspect ratio, a/b. Exact solution: solid line; approximate solution: dashed line.

First, the non-dimensional torsional stiffness, $\bar{H}_{11}$, evaluated using the co-location method and Fourier series approaches, see eqs. (7.52) and (7.54), respectively, are compared in fig. 7.24. Both solutions are in fair agreement for aspect ratios near unity, but the approximate solution significantly underpredicts the stiffness for higher aspect ratios. For a very thin strip, $a/b \to \infty$, $\bar{H}_{11} = 1/3 = 0.333$ for the exact solution, but $\bar{H}_{11} = 2/9 = 0.222$ for the approximate solution, a 33% error.

The maximum values of the shear stress components, τ_{12} and τ_{13}, are found at points **B** and **A**, respectively, at the middle of the two sides, see fig. 7.21. The approximate solution gives $ab^2|\tau_{12}^B|/M_1 = 4.5$ and $ab^2|\tau_{13}^A|/M_1 = 4.5\ b/a$. The exact solution is obtained from the series in eqs. (7.55). Figures 7.25 and 7.26 show the shear stresses at points **B** and **A**, respectively, as a function of the aspect ratio, a/b. The maximum shear stress occurs at point **B**, the mid-point of the section's long side. For a thin strip, $ab^2|\tau_{12}^B|/M_1 = 3$.

Large discrepancies are observed between the two solutions. The approximate solution obtained with the co-location method is not good enough to accurately estimate the stress distribution in the section.

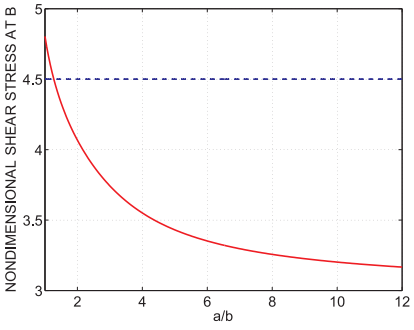

Fig. 7.25. Non-dimensional shear stress at point **B** versus aspect ratio a/b. Exact solution: solid line; approximate solution: dashed line.

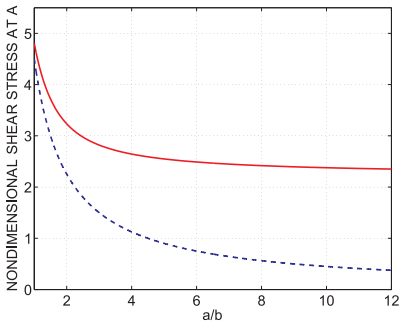

Fig. 7.26. Non-dimensional shear stress at point **A** versus aspect ratio a/b. Exact solution: solid line; approximate solution: dashed line.

7.3.4 Problems

Problem 7.8. Bar with circular section and semi-circular keyway
Consider a circular shaft of radius a with a semi-circular keyway of radius b, as depicted in fig. 7.27. The shaft is subjected to torsion. A stress function of the following form will be used

$$\phi = A(x_2^2 + x_3^2 - 2ax_2)\left[1 - \frac{b^2}{(x_2^2 + x_3^2)}\right],$$

where A is an unknown constant. *(1)* Verify that the proposed stress function satisfies the required boundary conditions. *(2)* Determine the stress function for this problem, *i.e.*, find the value of constant A. *(3)* Find the shear stress distribution $\tau_r = \tau_r(\alpha)$ and $\tau_\alpha = \tau_\alpha(\alpha)$ along the contour $\mathcal{C}_a$ of the shaft. *(4)* Find the shear stress distribution $\tau_r = \tau_r(\beta)$ and $\tau_\beta = \tau_\beta(\beta)$ along the contour $\mathcal{C}_b$ of the keyway. *(5)* Let $\tau_N = G\kappa_1 a$ be the shaft maximum shear stress *in the absence of keyway*. Find $\lim_{b\to 0} \tau_\alpha^A/\tau_N$ and $\lim_{b\to 0} \tau_\beta^B/\tau_N$. Comment on your results.

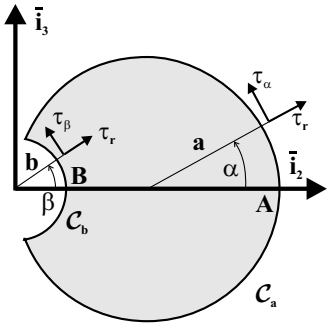

Fig. 7.27. Circular shaft with a circular keyway.

Problem 7.9. Torsion of bar with rectangular cross-section
A exact solution for the torsion of a bar with a rectangular cross-section depicted in fig. 7.21 is developed in section 7.3.3 using an open double trigonometric series. It is possible to develop a somewhat more efficient solution by assuming a trigonometric series solution in only one direction and an unknown function, $g_n(\eta)$, in the other. Consider the following single open series expansion for the stress function

$$\phi(\eta, \zeta) = \sum_{n=\text{odd}}^{\infty} g_n(\eta) \cos \alpha_n \zeta,$$

where $g_n(\eta)$ are unknown functions, $\alpha_n = n\pi/2$, $\eta = 2x_2/a$ is the non-dimensional coordinate along axis $\bar{\imath}_2$, and $\zeta = 2x_3/b$ is the non-dimensional coordinate along axis $\bar{\imath}_3$. Following the same approach used in section 7.3.3 and making use of the orthogonality of cosine functions, show that eq. (7.43) reduces to the following ordinary differential equations for $g_n(\eta)$

$$g_n'' - \beta_n^2 g_n = -\frac{Ga^2\kappa_1}{\alpha_n}(-1)^{(n-1)/2}, \quad \text{for n=odd}$$

where $\beta_n = \alpha_n a/b$, along with the boundary conditions $0 = g_n(\eta = \pm 1)$. Next, solve these equations, and after substituting in the above expression for $\phi(\eta, \zeta)$, show that

$$\phi(\eta,\zeta) = b^2 G\kappa_1 \sum_{n=\text{odd}}^{\infty} \frac{(-1)^{(n-1)/2}}{\alpha_n^3}\left[1 - \frac{\cosh\beta_n\eta}{\cosh\beta_n}\right]\cos\alpha_n\zeta$$

From this result, show that the non-dimensional torsional stiffness can be written as

$$\bar{H}_{11} = \frac{H_{11}}{Gab^3} = 2\sum_{n=\text{odd}}^{\infty}\left[\frac{1}{\alpha_n^4} - \frac{\tanh\beta_n}{\alpha_n^4\beta_n}\right] = \frac{1}{3} - 2\frac{1}{a/b}\sum_{n=odd}^{\infty}\frac{\tanh\beta_n}{\alpha_n^5}.$$

Note that $\sum_{n=odd}^{\infty} 1/n^4 = \pi^4/96$, and hence, $2\sum_{n=\text{odd}}^{\infty} 1/\alpha_n^4 = 1/3$. For a thin rectangular strip, $a/b \to \infty$ and $\bar{H}_{11} \to 1/3$. Finally, show that the shear stress at point **B** is given by

$$\frac{ab^2|\tau_B|}{M_1} = \frac{2}{\bar{H}_{11}}\sum_{n=\text{odd}}^{\infty}\left[\frac{1}{\alpha_n^2} - \frac{1}{\alpha_n^2\cosh\beta_n}\right] = \frac{1}{\bar{H}_{11}} - \frac{2}{\bar{H}_{11}}\sum_{n=odd}^{\infty}\frac{1}{\alpha_n^2\cosh\beta_n}.$$

Note that $\sum_{n=odd}^{\infty} 1/n^2 = \pi^2/8$, and hence, $2\sum_{n=\text{odd}}^{\infty} 1/\alpha_n^2 = 1$. The shear stress component at point **A** is given by

$$\begin{aligned}\frac{ab^2|\tau_A|}{M_1} =& \frac{2}{\bar{H}_{11}}\sum_{n=\text{odd}}^{\infty}\left[\frac{(-1)^{(n-1)/2}}{\alpha_n^2} - (-1)^{(n-1)/2}\frac{1-\tanh\beta_n}{\alpha_n^2}\right]\\ =& \frac{0.742454}{\bar{H}_{11}} - \frac{2}{\bar{H}_{11}}\sum_{n=odd}^{\infty}(-1)^{(n-1)/2}\frac{1-\tanh\beta_n}{\alpha_n^2}.\end{aligned}$$

Note that $\sum_{n=odd}^{\infty}(-1)^{(n-1)/2}/n^2 = 0.91596$, which is known as Catalan's constant. This particular arrangement of the equations for $\bar{H}_{11}$ and τ_A is done so that the series expressions can be more easily evaluated as a function of the sectional aspect ratio, a/b, as it approaches large values (at which $\tanh\ \beta_n \to 1$); in both cases the second term in the equations approaches zero. Note also the very fast convergence of all the series involved in this solution due to the powers of α_n appearing in the denominators.

7.4 Torsion of a thin rectangular cross-section

The torsion of a thin rectangular strip is an important problem that will form the basis for the analysis of beams with thin-walled cross-sections. An exact solution for the limiting case of a very thin rectangular strip can be easily developed. Consider the thin rectangular strip shown in fig. 7.28, where b is the long dimension of the cross-section, taken along axis $\bar{\imath}_3$, and t the thickness of the strip. If the thickness is much smaller than the length, *i.e.*, if $t \ll b$, it is reasonable to assume that both stress function and associated shear stress distributions will be nearly constant along axis $\bar{\imath}_3$. This will imply that $\partial\phi/\partial x_3 \approx 0$.

The term $\partial^2\phi/\partial x_3^2$ that appears in the governing equation for the stress function, eq. (7.43), now vanishes, and this governing equation reduces to the following ordinary differential equation,

$$\frac{\mathrm{d}^2\phi}{\mathrm{d}x_2^2} = -2G\kappa_1. \tag{7.56}$$

This equation is easily integrated to find $\phi(x_2) = -G\kappa_1 x_2^2 + C_1 x_2 + C_2$, where C_1 and C_2 are two integration constants. The boundary condition, eq. (7.45b), requires that $\phi(x_2 = \pm t/2) = 0$, which implies $C_1 = 0$ and $C_2 = G\kappa_1 t^2/4$. The stress function then becomes

$$\phi(x_2) = -G\kappa_1 \left(x_2^2 - \frac{t^2}{4} \right). \tag{7.57}$$

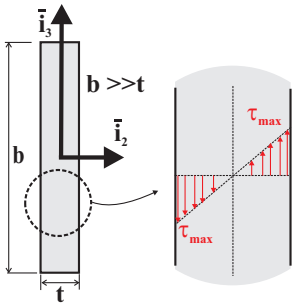

Fig. 7.28. Thin rectangular strip under torsion.

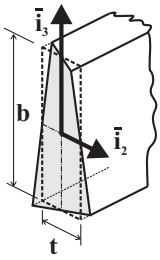

Fig. 7.29. Warping function for a thin rectangular strip.

The resulting torque is computed using eq. (7.48), to find

$$M_1 = 2 \int_{\mathcal{A}} \phi \, \mathrm{d}\mathcal{A} = -2G\kappa_1 \int_{-t/2}^{t/2} \left(x_2^2 - \frac{t^2}{4} \right) b \, \mathrm{d}x_2 = \frac{1}{3} G\kappa_1 b t^3.$$

This result reveals the torsional stiffness of the section, $H_{11} = M_1/\kappa_1$, as

$$H_{11} = \frac{1}{3} G b t^3. \tag{7.58}$$

The shear stress distribution now follows from eq. (7.41) as

$$\tau_{12} = \frac{\partial \phi}{\partial x_3} = 0, \quad \tau_{13} = -\frac{\partial \phi}{\partial x_2} = 2G\kappa_1 x_2 = \frac{6M_1}{bt^3} x_2. \tag{7.59}$$

This distribution is depicted in the right portion of fig. 7.28. The maximum shear stress occurs all along the long edges of the section, where $x_2 = \pm t/2$, and is of magnitude $|\tau^{\max}| = 3M_1/(bt^2)$.

The warping function, Ψ, can be determined by substituting the stress function solution, eq. (7.57), into eq. (7.42) to find two partial differential equations

$$\frac{\partial \Psi}{\partial x_2} = \frac{1}{G\kappa_1} \frac{\partial \phi}{\partial x_3} + x_3 = x_3, \quad \frac{\partial \Psi}{\partial x_3} = -\frac{1}{G\kappa_1} \frac{\partial \phi}{\partial x_2} - x_2 = x_2,$$

the solutions of which are $\Psi = x_3 x_2 + f(x_3)$ and $\Psi = x_2 x_3 + g(x_2)$, respectively; $f(x_3)$ and $g(x_2)$ are two arbitrary functions. Because the problem must have a unique

solution, the two expressions for Ψ must be equal. This is only possible if $f(x_3) = g(x_2) = 0$, leaving the warping function as $\Psi = x_2 x_3$. The axial displacement, $u_1(x_2, x_3)$, can be determined by substituting this result into eq. (7.32a) to find

$$u_1(x_2, x_3) = \Psi(x_2, x_3)\kappa_1 = \kappa_1 x_2 x_3. \tag{7.60}$$

As discussed in section 7.3.1, the warping function for a rectangular section must be antisymmetric with respect to both axes $\bar{\imath}_2$ and $\bar{\imath}_3$. The above solution does indeed satisfy this antisymmetry requirement, as illustrated in fig. 7.29.

7.5 Torsion of thin-walled open sections

The results presented in the previous section are readily extended to thin-walled open sections of arbitrary shape. The solution developed for the thin rectangular strip is based on the assumption that the gradient of the stress function vanishes in the direction tangential to the thin wall; for the thin rectangular strip shown in fig. 7.28, this means along axis $\bar{\imath}_3$. Of course, had the thin strip been rotated by 90 degrees, the gradient of the stress function would have been assumed to vanish along axis $\bar{\imath}_2$.

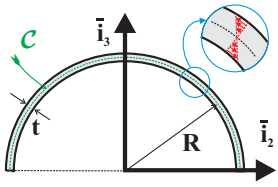

Fig. 7.30. Semi-circular thin-walled open section.

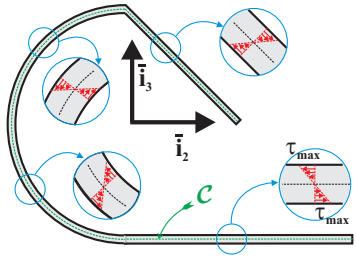

Fig. 7.31. Thin-walled open section composed of several curved.

More generally, the gradient of the stress function should vanish along the local tangent to the section's thin wall, and the corresponding shear stress distribution will then be linear through the wall thickness. For thin-walled open sections, the geometry of the cross-section can be represented by an open curve, $\mathcal{C}$, drawn along the wall's mid-thickness, as illustrated in fig. 7.30 for a semi-circular, thin-walled section.

The developments of the previous section still apply to a generally curved, thin-walled open section, and by extension of eq. (7.58), the torsional stiffness of such section becomes

$$H_{11} = G\,\frac{\ell t^3}{3}, \tag{7.61}$$

where ℓ is the length of curve $\mathcal{C}$ and t the wall thickness. For instance, the torsional stiffness of the semi-circular section shown in fig. 7.30 is $H_{11} = G\,\pi R t^3/3$.

For the thin rectangular section, the shear stress τ_{12} vanishes, leaving τ_{13} as the sole shear stress component, see eq. (7.59). For the present problem, the only non-vanishing stress component is the *tangential shear stress*, τ_s, acting in the direction tangent to curve $\mathcal{C}$. Here again, the shear stress is not uniform across the thickness, but instead, varies linearly from zero at the midline to maximum positive and negative values at the opposite edges of the wall, a distance $\pm t/2$ from the midline. At these points, the magnitude of the shear stress is

$$\tau_s^{\max} = Gt\,\kappa_1. \tag{7.62}$$

The maximum shear stress can also be expressed in terms of the applied torque as

$$\tau_s^{\max} = \frac{3M_1}{\ell t^2}. \tag{7.63}$$

A more general thin-walled open section could be composed of a number of straight and curved segments, such as the situation illustrated in fig. 7.31. In this case, the torsional stiffness of the cross-section is the sum of the torsional stiffnesses of the individual segments and can be expressed as,

$$H_{11} = \sum_i H_{11}^{(i)} = \frac{1}{3}\sum_i G_i \ell_i t_i^3, \tag{7.64}$$

where G_i, ℓ_i and t_i are the shear modulus, length and thickness of the i^{th} segment, respectively. The shear stress along the edge of each segment is still given by eq. (7.62), where κ_1 is the twist rate of the cross-section. Hence, the maximum shear stress will be found in the segment featuring the largest thickness

$$\tau_s^{\max} = Gt_{\max}\frac{M_1}{H_{11}}, \tag{7.65}$$

where $t_{\max}$ is the thickness of the segment with the largest thickness.

Warping of a thin-walled open section is more complex and involves not only the warping behavior of a thin rectangular strip described in section 7.4 and defined by eq. (7.60), but it also includes a much larger warping of the overall cross-section. The warping of open thin-walled sections will be described in chapter 8 in section 8.7.

Example 7.3. Torsion of thin-walled section

Consider, as an example, the C-channel shown in fig. 7.32. The torsional stiffness of the section is given by eq. (7.64) as

$$H_{11} = \frac{G}{3}\left(bt_f^3 + ht_w^3 + bt_f^3\right) = \frac{G}{3}\left(ht_w^3 + 2bt_f^3\right). \tag{7.66}$$

The tangential shear stresses at the outer edges of the wall are given by eq. (7.62) as $\tau_w = Gt_w\kappa_1 = Gt_wM_1/H_{11}$ and $\tau_f = Gt_f\kappa_1 = Gt_fM_1/H_{11}$, for the stresses in the web and flanges, respectively. The maximum shear stress will be found in the segment featuring the maximum thickness.

7.5.1 Problems

Problem 7.10. Torsional stiffness of a section with variable thickness
Figure 7.32 depicts the cross-section of a thin-walled beam with different thicknesses. For this problem, assume that $t_w = t$ and $t_f = 2t$. *(1)* Find the torsional stiffness of the section. *(2)* Find the magnitude and location of the maximum shear stress if the section is subjected to a torque Q. *(3)* Sketch the distribution of shear stress through the thickness of the wall for the two regions with different thicknesses.

Problem 7.11. Torsional stiffness of a C-section
Consider the thin-walled, C-section of a beam depicted in fig. 7.32. The dimensions of the section are $b = 20$ mm, $h = 50$ mm, $t_w = 4$ mm and $t_f = 5$ mm. *(1)* Find the torsional stiffness of the section. *(2)* Compute the maximum shear stress in the section due to an applied torque Q. *(3)* Indicate the location of the maximum shear stress. *(4)* Sketch the distribution of shear stress through the thickness of the wall. The shear modulus for the material is $G = 30$ GPa and the applied torque is $Q = 120$ N·m.

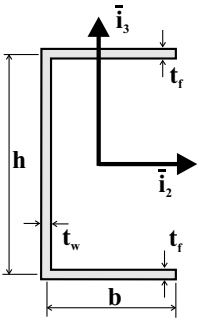

Fig. 7.32. A thin-walled C-channel section

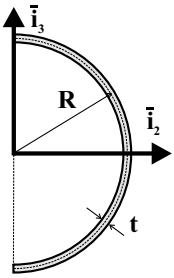

Fig. 7.33. Semi-circular open cross-section.

Problem 7.12. Torsional stiffness of a semi-circular section
Figure 7.33 depicts the thin-walled, semi-circular open cross-section of a beam. The wall thickness is t, and the material Young's and shear moduli are E and G, respectively. *(1)* Find the torsional stiffness of the section. *(2)* Find the distribution of shear stress due to an applied torque Q. *(3)* Indicate the location and magnitude of the maximum shear stress, $Rt^2\tau_{\max}/Q$.

Problem 7.13. Torsional stiffness of an "H" shaped cross-section
Figure 7.34 depicts the cross-section of a thin-walled beam with what is sometimes called an "H" shaped cross-section. For this problem, assume that $h_1 = b/2$ and $h_2 = b/4$. *(1)* Find the torsional stiffness of the section. *(2)* Find the magnitude and location of the maximum shear stress if the section is subjected to a torque Q. *(3)* Sketch the distribution of shear stress through the thickness of the wall.

Problem 7.14. Torsional stiffness of a "Y" shaped cross-section
Figure 7.35 depicts the "Y" shaped cross-section of a thin-walled beam. The horizontal leg of the cross-section has a thickness $2t$, whereas the other two legs are of thickness t. *(1)* Determine the torsional stiffness of the section. *(2)* Determine the magnitude and location of the maximum shear stress if a torque Q is applied to the beam. *(3)* Sketch the shear stress distribution through the wall thickness.

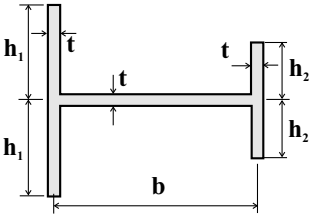

Fig. 7.34. "H" cross-section of a thin-walled beam.

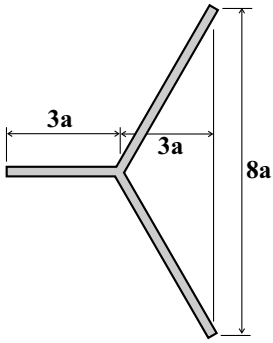

Fig. 7.35. "Y" cross-section of a thin-walled beam.